Journal of the Mechanics and Physics of Solids 56 (2008) 3224–3241

Contents lists available at ScienceDirect

Journal of the Mechanics and Physics of Solids

journal homepage: www.elsevier.com/locate/jmps

Mechanics of hydrogen storage in carbon nanotubes

Y.L. Chen [a], B. Liu [a,*], J. Wu [a], Y. Huang [b,c,*], H. Jiang [d], K.C. Hwang [a]

[a] FML, Department of Engineering Mechanics, Tsinghua University, Beijing 100084, China
[b] Department of Civil and Environmental Engineering, Northwestern University, Evanston, IL 60208, USA
[c] Department of Mechanical Engineering, Northwestern University, Evanston, IL 60208, USA
[d] Department of Mechanical and Aerospace Engineering, Arizona State University, Tempe, AZ 85287, USA

ARTICLE INFO

Article history:
Received 23 April 2008
Received in revised form
12 July 2008
Accepted 17 July 2008

Keywords:
Hydrogen storage
Carbon nanotube
Continuum model
Analytical solution
Atomistic simulations

ABSTRACT

A continuum mechanics model is established for hydrogen storage in single- and multi-wall carbon nanotubes (CNTs) and the bundle of single-wall CNTs. The model accounts for the deformation of CNTs, and van der Waals interactions among hydrogen molecules and between hydrogen and carbon atoms. The analytical expressions of hydrogen storage (number of hydrogen molecules per unit volume) in CNTs are obtained, and are validated by atomistic simulations. CNTs are categorized as tiny, small, medium and large CNTs; tiny CNTs cannot achieve the goals of hydrogen storage (62 kg/m^3 and 6.5 wt% of hydrogen set by the US Department of Energy) without fracture; small CNTs are strained during hydrogen storage; medium CNTs can achieve the above goals without the strain and do not self collapse; and large CNTs may self collapse upon the release of hydrogen.

1. Introduction

Hydrogen is the cleanest vector of energy. Vehicles propelled by electric motors supplied by hydrogen fuel cells may reach zero emission, and therefore do not cause urban pollution. One challenge in this development is the storage and release of hydrogen.

Carbon nanotubes (CNTs) display superior mechanical properties and have many potential applications. One of them is the hydrogen storage (Darkrim et al., 2002) because

(i) carbon is a good adsorbent for gases; and
(ii) CNTs are microporous carbon macromolecules with high specific surface, and have the potential to adsorb hydrogen in their nanostructures (Darkrim et al., 2002).

Dillon et al. (1997) measured the hydrogen adsorption in CNTs in order to evaluate the hydrogen adsorption amount delivered during the gas desorption, and concluded that CNTs were promising for hydrogen storage. Liu et al. (1999) investigated the hydrogen adsorption in CNTs at room temperature and reached the same conclusion. Darkrim and Levesque (1998, 2000) computed hydrogen adsorption in opened CNTs for a wide range of pressure and temperature, and optimized the tube diameters and the inter-tube spacing to achieve high adsorptive property.

The adsorption is expressed as a unit of quantity of gas with respect to a unit of quantity of adsorbent. Experiments have shown large scatting in the achievable hydrogen storage, ranging from 0.25 to 11 wt% (e.g., Dillon et al., 1997; Liu et al.,

* Corresponding authors.
E-mail addresses: liubin@tsinghua.edu.cn (B. Liu), y-huang@northwestern.edu (Y. Huang).

0022-5096/$ - see front matter © 2008 Elsevier Ltd. All rights reserved.
doi:10.1016/j.jmps.2008.07.007

1999; Ye et al., 1999; Rajalakshmi et al., 2000; Wu et al., 2000; Dai et al., 2002). Multi-wall CNTs doped with Li, Kt and Pd may achieve higher hydrogen storage, ranging from 1.8 to 20 wt% (e.g., Chen et al., 1999; Yang, 2000; Mu et al., 2006). Many factors may be responsible for the large scatting in experimental data, such as the defects in CNTs, and opened or closed CNTs. The goals of hydrogen storage set by the US Department of Energy are 62 kg H_2/m^3 and 6.5 wt% (Dillon et al., 1997).

The purpose of this paper is to establish a simple mechanics model of hydrogen storage in CNTs. The model provides the analytical relation between the hydrogen storage (number of hydrogen molecules per unit volume) and the internal pressure in the CNT for single-, double- and triple-wall CNTs and bundle of single-wall CNTs. For each type (single-, double-, triple-wall, and bundle), CNTs can be categorized as tiny, small, medium and large CNTs, which, upon reaching the above goals of hydrogen storage (and then release of hydrogen), will experience fracture, strain, no strain (and do not self collapse) and self collapse, respectively. The model, which is validated by atomistic simulations, also provides the analytical relation between the maximum hydrogen storage and CNT radius.

The paper is structured as follows. The interatomic potentials for carbon and for van der Waals interactions are given in Section 2. The mechanics models of hydrogen storage are established in Sections 3–5 for single-wall CNTs, their bundles, and multi-wall CNTs, respectively, and are validated by atomistic simulations. The goals of hydrogen storage in CNTs are discussed in Section 6.

2. Interatomic potentials

Brenner et al. (2002) established the second-generation interatomic potential for carbon as

$$V(r_{ij},\theta_{ijk};\ k\neq i,j)=V_{\mathrm{R}}(r_{ij})-B_{ij}V_{\mathrm{A}}(r_{ij}), \tag{2.1}$$

where r_{ij} is the distance between atoms i and j, $V_{\mathrm{R}}(r)=(1+Q/r)Ae^{-\alpha r}f_{\mathrm{c}}(r)$ and $V_{\mathrm{A}}(r)=\sum_{n=1}^{3}B_n e^{-\beta_n r}f_{\mathrm{c}}(r)$ are the repulsive and attractive pair terms (i.e., depending only on r_{ij}), A, Q, α, B_n and β_n are constants, f_{c} is the cut-off function, and the multi-body coupling parameter $B_{ij}=[1+\sum_{k(\neq i,j)}G(\cos\theta_{ijk})f_{\mathrm{c}}(r_{ik})]^{-1/2}$ depends on the bond angle θ_{ijk} between i–j and i–k via the function G.

The van der Waals interactions between a carbon atom and a hydrogen molecule or between two hydrogen molecules are characterized by the Lennard–Jones 6-12 potential

$$V_{\mathrm{LJ}}=4\varepsilon\left(\frac{\sigma^{12}}{r_{ij}^{12}}-\frac{\sigma^{6}}{r_{ij}^{6}}\right), \tag{2.2}$$

where r_{ij} is the distance between atoms (and molecules), σ^{12}/r_{ij}^{12} and σ^{6}/r_{ij}^{6} represent the repulsive and attractive terms, respectively. For hydrogen molecules, $\varepsilon_{\mathrm{H_2-H_2}}=3.11\times10^{-3}$ eV and $\sigma_{\mathrm{H_2-H_2}}=0.296$ nm (Gu et al., 2001). For a carbon atom and a hydrogen molecule, the Lorentz–Berthelet mixing rule (e.g., Allen and Tildesley, 1987) gives $\varepsilon_{\mathrm{C-H_2}}=\sqrt{\varepsilon_{\mathrm{C-C}}\cdot\varepsilon_{\mathrm{H_2-H_2}}}=2.73\times10^{-3}$ eV and $\sigma_{\mathrm{C-H_2}}=\frac{1}{2}(\sigma_{\mathrm{C-C}}+\sigma_{\mathrm{H_2-H_2}})=0.319$ nm, where $\varepsilon_{\mathrm{C-C}}=2.39\times10^{-3}$ eV and $\sigma_{\mathrm{C-C}}=0.342$ nm (Gu et al., 2001; Frankland et al., 2003).

3. Hydrogen storage in single-wall CNTs

3.1. Atomistic model of hydrogen storage in single-wall CNTs

Fig. 1(a) shows the atomistic model used in the prior molecular dynamics simulations of hydrogen storage in single-wall CNTs (e.g., Cheng et al., 2001, 2004; Gu et al., 2001; Dodziuk and Dolgonos, 2002). The covalent bonds between carbon atoms on the CNT are characterized by the interatomic potential in Eq. (2.1). The carbon atoms interact with the hydrogen molecules inside the CNT via the van der Waals forces obtained from Eq. (2.2) with $\varepsilon_{\mathrm{C-H_2}}=2.73\times10^{-3}$ eV and $\sigma_{\mathrm{C-H_2}}=0.319$ nm, while hydrogen molecules also interact via the van der Waals forces with $\varepsilon_{\mathrm{H_2-H_2}}=3.11\times10^{-3}$ eV and $\sigma_{\mathrm{H_2-H_2}}=0.296$ nm. Both carbon atoms and hydrogen molecules are discrete in the atomistic model.

The atomic-scale finite element method (AFEM) (Liu et al., 2004a, 2005), which is an effective and robust atomistic simulation method based on the second-generation interatomic potential for hydrocarbons (Brenner et al., 2002), is adopted. It models each atom or molecule as a node, and accurately describes the C–C covalent bonds, and C–H_2 and H_2–H_2 van der Waals interactions. The hydrogen molecules are randomly added inside the CNT. The system is then relaxed to minimize the total energy (in the covalent bonds and due to van der Waals interactions), which determines the positions of carbon atoms and hydrogen molecules.

Fig. 2 shows the internal pressure p in the CNT versus the percentage of change of CNT radius, $\Delta R/R$, for a (5,5) CNT. Here the new radius of CNT $R+\Delta R$ is obtained by averaging the positions of carbon atoms in the radial direction. The pressure is the ratio of total force (in the radial direction) of all carbon atoms to the current area of the CNT surface. The nonlinear $p\sim\Delta R/R$ relation results from the nonlinear atomistic interactions. The peak pressure corresponds to the CNT fracture (breakage of a C–C bond). The maximum hydrogen storage at the peak pressure is 25.6 hydrogen molecules/nm^3. This gives 85.0 kg H_2/m^3 and 3.75 wt% for the (5,5) CNT, which exceeds the goal 62 kg H_2/m^3 but falls short to reach the other goal 6.5 wt% of hydrogen storage [set by the US Department of Energy, see Dillon et al. (1997)]. Therefore, large CNTs (large radius) are needed for hydrogen storage.

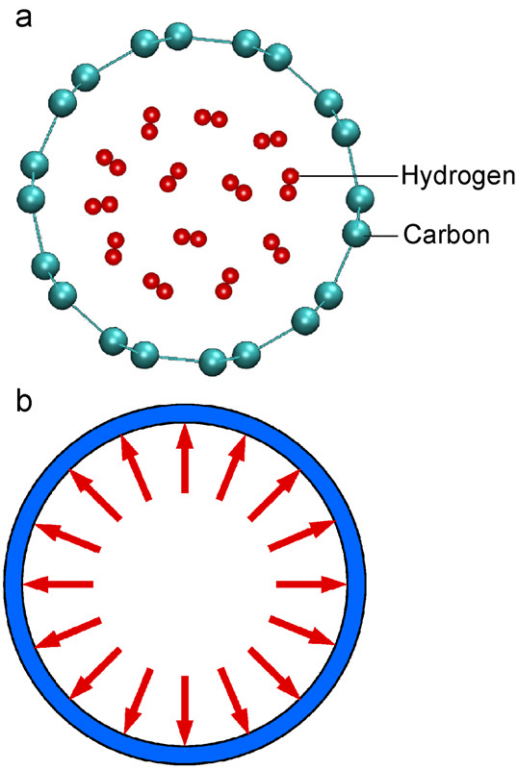

Fig. 1. Schematic diagrams of hydrogen storage in single-wall carbon nanotubes: (a) atomistic model (AFEM), in which carbon atoms and hydrogen molecules are discrete; (b) continuum model, in which carbon nanotubes are represented by a continuum shell, while hydrogen molecules are represented by the internal pressure.

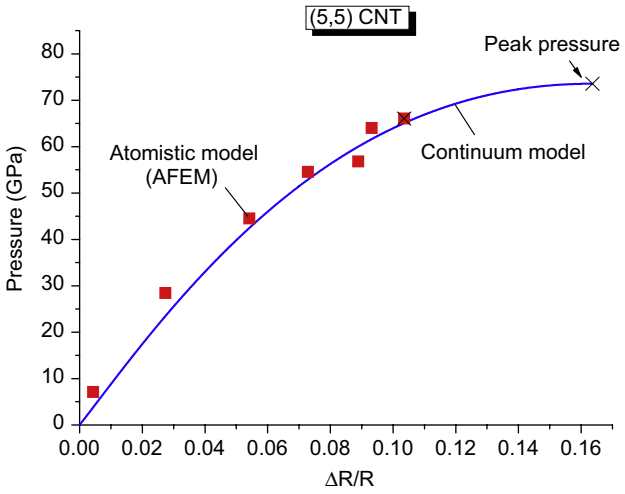

Fig. 2. The pressure inside the single-wall (5,5) carbon nanotube versus the percentage change of nanotube radius for the atomistic (AFEM) and continuum models. The peak pressure is denoted.

3.2. Continuum model of hydrogen storage in single-wall CNTs

For large CNTs the atomistic model becomes less effective. The continuum model is developed in this section to establish a simple, analytical expression for hydrogen storage in single-wall CNTs. Fig. 1(b) shows the continuum model in Section 3.2.1 to represent the CNT as a continuum shell. The hydrogen molecules in the CNT are represented by the internal pressure p. A simple analytical relation is established in Section 3.2.2 to give the average spacing between hydrogen

molecules in the CNT in terms of the internal pressure p. A similar relation is established in Section 3.2.3 to relate the average spacing between the CNT wall and nearest hydrogen molecules to the internal pressure p. As p increases, the H_2–H_2 spacing and C–H_2 spacing decrease, but the CNT radius increases, which lead to the increasing hydrogen storage in Section 3.3.4.

3.2.1. Continuum modeling of the CNT

The CNT is modeled as a nonlinear continuum thin shell (Fig. 1(b)), where the nonlinearity results from the large stretch of C–C bonds due to hydrogen storage, as characterized by the interatomic potential, Eq. (2.1). Zhang et al. (2002, 2004) and Wu et al. (2008) established a continuum theory for CNTs directly from the interatomic potential, similar to the previously developed Virtual-Internal-Bond model for cohesive fracture (Gao and Klein, 1998) but accounting for the atomic structure and multi-body atomistic interactions. This atomistic-based continuum theory is briefly summarized in the following.

The Cauchy–Born rule (Born and Huang, 1954) equates the strain energy at continuum level to the energy stored in atomic bonds. The atoms subjected to a homogeneous deformation move according to a single mapping $\boldsymbol{F}=\partial\boldsymbol{x}/\partial\boldsymbol{X}$ from the initial, undeformed to the current, deformed configurations, where $\boldsymbol{X}$ and $\boldsymbol{x}$ denote positions of a material point in the initial and current configurations, respectively. A bond between a pair of atoms i and j in the initial configuration is described by a vector $\boldsymbol{r}_{ij}^{(0)}=r_0\boldsymbol{n}$, where r_0 is the initial bond length and $\boldsymbol{n}$ is the unit vector along the initial bond direction. For a simple Bravais lattice, the deformed bond is $\boldsymbol{r}_{ij}=\boldsymbol{F}\cdot\boldsymbol{r}_{ij}^{(0)}$, which has the length $r_{ij}=\sqrt{\boldsymbol{r}_{ij}^{(0)}\cdot(\boldsymbol{I}+2\boldsymbol{E})\cdot\boldsymbol{r}_{ij}^{(0)}}=r_0\sqrt{\boldsymbol{n}\cdot(\boldsymbol{I}+2\boldsymbol{E})\cdot\boldsymbol{n}}$, where $\boldsymbol{E}=\frac{1}{2}(\boldsymbol{F}^{\mathrm{T}}\cdot\boldsymbol{F}-\boldsymbol{I})$ is the Green strain tensor and $\boldsymbol{I}$ is the second-order identity tensor. The single mapping $\boldsymbol{F}$ ensures the equilibrium of atoms for a simple Bravais lattice.

A CNT, however, is a Bravais multi-lattice that can be decomposed into two simple Bravais sub-lattices as shown by the open and solid circles in Fig. 3. Each sub-lattice follows the single mapping $\boldsymbol{F}$, but the two sub-lattices may have a shift $\boldsymbol{\zeta}$ (Fig. 3) to be determined from the equilibrium of atoms. The deformed bond (between atoms from two different sub-lattices) then becomes

$$\boldsymbol{r}_{ij}=\boldsymbol{F}\cdot\boldsymbol{r}_{ij}^{(0)}+\boldsymbol{\zeta}. \tag{3.1}$$

This gives the bond length r_{ij} and angle θ_{ijk} in terms of the Green strain $\boldsymbol{E}$ as

$$r_{ij}^2=r_0^2(\delta_{\alpha\beta}+2E_{\alpha\beta})(n_\alpha+\eta_\alpha)(n_\beta+\eta_\beta), \tag{3.2}$$

$$\cos\,\theta_{ijk}=\frac{r_0^2}{r_{ij}r_{ik}}(\delta_{\alpha\lambda}+2E_{\alpha\lambda})(n_\alpha^{(1)}+\eta_\alpha)(n_\lambda^{(2)}+\eta_\lambda), \tag{3.3}$$

where $\boldsymbol{\eta}=(1/r_0)\boldsymbol{F}^{-1}\cdot\boldsymbol{\zeta}$, and the superscripts 1 and 2 denote the two bonds in a bond angle.

The strain energy density W in the continuum theory is obtained from the interatomic potential V via the Cauchy–Born rule,

$$W=\frac{1}{2}\frac{\sum V(r_{ij},\theta_{ijk};\ k\neq i,j)}{A_0}, \tag{3.4}$$

where the summation is for three nearest-neighbor atoms, the factor one half results from the equi-partition of bond energy, and A_0 is the area of CNT per atom. It is important to point out that the above equation accounts for the effect of second-nearest-neighbor atoms via the bond angle θ_{ijk}. The shift vector $\boldsymbol{\zeta}$ (or $\boldsymbol{\eta}$) is determined numerically from the

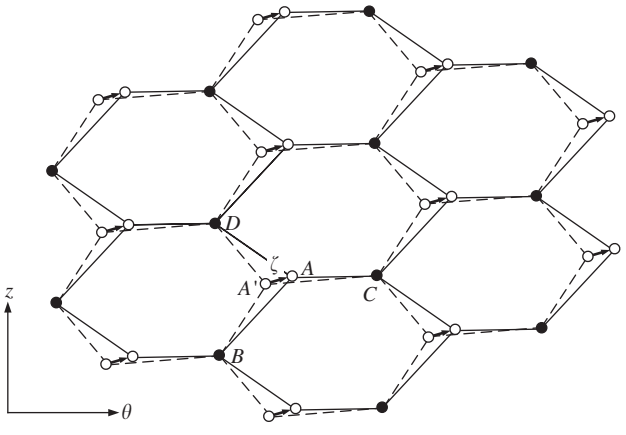

Fig. 3. The decomposition of a hexagonal lattice to two triangular sub-lattices. A shift vector $\boldsymbol{\zeta}$ between two sub-lattices is introduced to ensure the equilibrium of atoms.

equilibrium of atoms as

$$\frac{\partial W}{\partial \boldsymbol{\zeta}} = \frac{\partial W}{\partial \boldsymbol{\eta}} = 0. \tag{3.5}$$

The second Piola–Kirchhoff stress $\boldsymbol{T}$ is related to the Green strain $\boldsymbol{E}$ by

$$\boldsymbol{T}t = \frac{\partial W}{\partial \boldsymbol{E}}, \tag{3.6}$$

where the stress appears together with the CNT thickness t since the strain energy density W in Eq. (3.4) is the strain energy per unit area, and is also obtained numerically. The pressure in the current configuration is obtained from the equilibrium as

$$p = \frac{T_{\theta\theta} t}{R(1+\varepsilon_{zz})}, \tag{3.7}$$

where the (nominal) strain ε_{zz} in the axial direction is determined numerically from $T_{zz} = 0$.

Fig. 2. shows the internal pressure p in the CNT versus the percentage of change of CNT radius, $\Delta R/R$, for the (5,5) CNT. The continuum model gives the same curve as the atomistic model, which means that the CNT can indeed be represented by a thin shell in the continuum model. Only the peak pressure (after which the stress–strain curve displays the softening behavior) given by the continuum model is slightly higher than the atomistic model. This is because the CNT is subjected to the uniform internal pressure in the continuum model, while the atomistic model is nonuniform (due to hydrogen molecules), which may trigger earlier bond breakage.

For small deformation the above continuum model becomes linear elastic isotropic, and therefore simple, analytical solution. Its constitutive model becomes (Huang et al., 2006)

$$\begin{aligned}(\sigma_{\theta\theta}+\sigma_{zz})t &= \frac{1}{\sqrt{3}}\left(\frac{\partial^2 V}{\partial r_{ij}^2}\right)_0 (\varepsilon_{\theta\theta}+\varepsilon_{zz}),\\ (\sigma_{\theta\theta}-\sigma_{zz})t &= \frac{B}{8\sqrt{3}}(\varepsilon_{\theta\theta}-\varepsilon_{zz}),\end{aligned} \tag{3.8}$$

where V is the interatomic potential in Eq. (2.1), the subscript "0" denotes the values at the initial equilibrium state, $r_{ij} = r_0$ and $\theta_{ijk} \approx 120^\circ$, B is given in terms of the derivatives of the interatomic potential at the initial equilibrium state as

$$\begin{aligned}B = \frac{3(1-A)^2}{r_0^2}&\left[4\left(\frac{\partial V}{\partial \cos\theta_{ijk}}\right)_0 + 6\left(\frac{\partial^2 V}{\partial \cos\theta_{ijk}\,\partial \cos\theta_{ijk}}\right)_0 - 3\left(\frac{\partial^2 V}{\partial \cos\theta_{ijk}\,\partial \cos\theta_{ijl}}\right)_0\right]\\ &+ 4(1+A)^2\left(\frac{\partial^2 V}{\partial r_{ij}^2}\right)_0 - 12\frac{(1-A^2)}{r_0}\left(\frac{\partial^2 V}{\partial r_{ij}\,\partial \cos\theta_{ijk}}\right)_0,\end{aligned} \tag{3.9}$$

and

$$A = 1 - \frac{8r_0^2\left(\frac{\partial^2 V}{\partial r_{ij}^2}\right)_0 + 12r_0\left(\frac{\partial^2 V}{\partial r_{ij}\,\partial \cos\theta_{ijk}}\right)_0}{12\left(\frac{\partial V}{\partial \cos\theta_{ijk}}\right)_0 + 4r_0^2\left(\frac{\partial^2 V}{\partial r_{ij}^2}\right)_0 + 18\left(\frac{\partial^2 V}{\partial \cos\theta_{ijk}\,\partial \cos\theta_{ijk}}\right)_0 - 9\left(\frac{\partial^2 V}{\partial \cos\theta_{ijk}\,\partial \cos\theta_{ijl}}\right)_0 + 12r_0\left(\frac{\partial^2 V}{\partial r_{ij}\,\partial \cos\theta_{ijk}}\right)_0}. \tag{3.10}$$

The equilibrium bond length is obtained by minimizing the potential $\partial V/\partial r_{ij}|_{r_{ij}=r_0,\,\theta_{ijk}\approx 120^\circ} = 0$ as $r_0 = 0.142$ nm for the second-generation interatomic potential (Brenner et al., 2002). The Young's modulus E of the CNT is obtained from Eq. (3.8) as

$$Et = \frac{2/\sqrt{3}}{\frac{1}{(\partial^2 V/\partial r_{ij}^2)_0} + \frac{8}{B}}, \tag{3.11}$$

where the Young's modulus appears together with the CNT thickness t since the strain energy density W in Eq. (3.4) is the strain energy per unit area. For small deformation, Eq. (3.7) gives the following approximate but analytical relation between the change of CNT radius ΔR and the internal pressure p (e.g., Timoshenko and Goodier, 1969)

$$\Delta R \approx \frac{pR^2}{Et} = \frac{\sqrt{3}}{2}pR^2\left[\frac{1}{(\partial^2 V/\partial r_{ij}^2)_0} + \frac{8}{B}\right]. \tag{3.12}$$

The above equation is approximate but analytical, contrary to the numerical but accurate solution in Eq. (3.7). Similarly, both the numerical (but accurate) and analytical (but approximate) solutions are also obtained for continuum models in the following.

3.2.2. Continuum modeling of hydrogen molecules

The average spacing between hydrogen molecules, which is an important parameter in hydrogen storage, is obtained analytically in terms of the pressure p in this section. The Virial stress widely used in molecular dynamics simulations gives the stress tensor at the location $\boldsymbol{r}_i$ of particle i as (McLellan, 1974; Tsai, 1979; Rowlinson and Widom, 1982)

$$\sigma = \frac{1}{\Omega}\left(-m_i \dot{\boldsymbol{u}}_i \dot{\boldsymbol{u}}_i + \frac{1}{2}\sum_{j(\neq i)} \boldsymbol{r}_{ij}\boldsymbol{f}_{ij}\right), \tag{3.13}$$

where Ω is average volume per particle, m_i and $\dot{\boldsymbol{u}}_i$ are the mass and velocity of particle i, respectively, $\boldsymbol{r}_{ij} = \boldsymbol{r}_j - \boldsymbol{r}_i$ is the interatomic relative position vector in the current configuration, $\boldsymbol{f}_{ij}$ is the interparticle force applied on particle i by particle j, and the summation is for all particles interacting with particle i. For the pair potential such as Lennard–Jones potential in Eq. (2.2) that depends only on the length $r_{ij} = |\boldsymbol{r}_{ij}|$,

$$\boldsymbol{f}_{ij} = \frac{\partial V_{\mathrm{LJ}}}{\partial \boldsymbol{r}_{ij}} = \frac{\mathrm{d}V_{LJ}}{\mathrm{d}r_{ij}}\frac{\boldsymbol{r}_{ij}}{r_{ij}}, \tag{3.14}$$

which is parallel to $\boldsymbol{r}_{ij}$. For the system at relatively low temperature, the kinetic energy can be omitted, and the Virial stress in Eq. (3.13) then becomes

$$\sigma = \frac{1}{2\Omega}\sum_{j(\neq i)} \frac{1}{r_{ij}}\frac{\mathrm{d}V_{\mathrm{LJ}}}{\mathrm{d}r_{ij}}\boldsymbol{r}_{ij}\boldsymbol{r}_{ij}. \tag{3.15}$$

The internal pressure is

$$p = -\frac{1}{6\Omega}\sum_{j(\neq i)} r_{ij}\,\frac{\mathrm{d}V_{\mathrm{LJ}}}{\mathrm{d}r_{ij}}. \tag{3.16}$$

For the limit of most closely packed hydrogen (AB stacking) illustrated in Fig. 4, there are 12 molecules surrounding each molecule, and their spacing is denoted by $d_{\mathrm{H_2-H_2}}$. The volume per hydrogen molecule is

$$\Omega = \frac{\sqrt{2}}{2} d^3_{\mathrm{H_2-H_2}}. \tag{3.17}$$

For the Lennard–Jones potential, Eq. (3.16) gives the following analytical relation to determine the spacing between hydrogen molecules $d_{\mathrm{H_2-H_2}}$ in terms of the internal pressure p:

$$p = \frac{48\sqrt{2}\varepsilon_{\mathrm{H_2-H_2}}}{\sigma^3_{\mathrm{H_2-H_2}}}\left[2\left(\frac{\sigma_{\mathrm{H_2-H_2}}}{d_{\mathrm{H_2-H_2}}}\right)^{15} - \left(\frac{\sigma_{\mathrm{H_2-H_2}}}{d_{\mathrm{H_2-H_2}}}\right)^{9}\right]. \tag{3.18}$$

The spacing $d_{\mathrm{H_2-H_2}}$ is $\sqrt[6]{2}\sigma_{\mathrm{H_2-H_2}}$ at the vanishing pressure $p = 0$, and decreases as the pressure p increases, as shown in Fig. 5 for the (5,5) CNT. The atomistic model, also shown in Fig. 5, agrees very well with Eq. (3.18), and therefore validates this relation established from the Virial stress.

Eq. (3.18) cannot be solved analytically to give the spacing $d_{\mathrm{H_2-H_2}}$ in terms of the pressure. An approximate but analytical expression can be obtained by neglecting $(\sigma_{\mathrm{H_2-H_2}}/d_{\mathrm{H_2-H_2}})^9$ in Eq. (3.18) since the repulsive term $(\sigma_{\mathrm{H_2-H_2}}/d_{\mathrm{H_2-H_2}})^{15}$ dominates as the internal pressure increases. The spacing $d_{\mathrm{H_2-H_2}}$ can then be approximated by

$$d_{\mathrm{H_2-H_2}} \approx \left(\frac{96\sqrt{2}\varepsilon_{\mathrm{H_2-H_2}}\sigma^{12}_{\mathrm{H_2-H_2}}}{p}\right)^{1/15}. \tag{3.19}$$

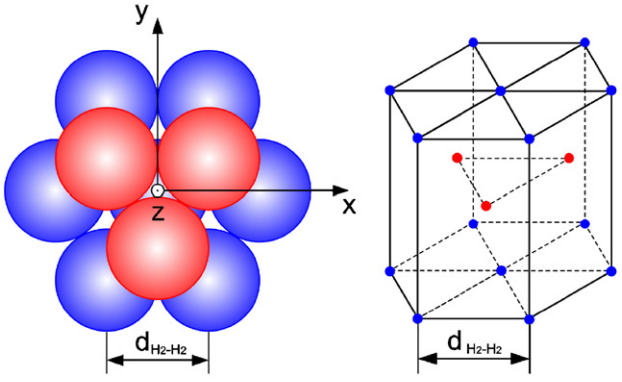

Fig. 4. Schematic diagrams of closely packed hydrogen molecules.

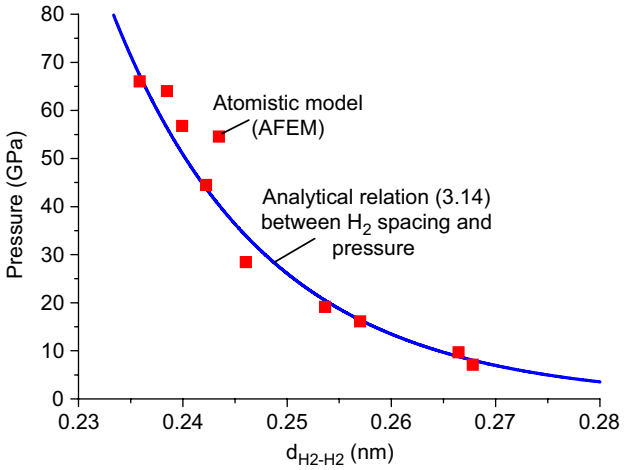

Fig. 5. The pressure inside the single-wall (5,5) carbon nanotube versus the equilibrium spacing between hydrogen molecules inside the nanotube. The results are shown for both the continuum model [Eq. (3.18)] and atomistic model (AFEM).

3.2.3. *Continuum model of interactions between the CNT and hydrogen molecules*

The average spacing d_{C-H_2} between the CNT wall and nearest hydrogen molecules, which is another important parameter in hydrogen storage, is obtained analytically in terms of the pressure p in this section. Jiang et al. (2006) established a cohesive law between a CNT and polymer molecules due to van der Waals interactions. By replacing polymer molecules with H_2, it is also applicable to interactions between a CNT and hydrogen molecules

$$p = 2\pi\Omega^{-1}\rho_C\varepsilon_{C-H_2}\sigma_{C-H_2}^2\left[\frac{2}{5}\left(\frac{\sigma_{C-H_2}}{d_{C-H_2}}\right)^{10} - \left(\frac{\sigma_{C-H_2}}{d_{C-H_2}}\right)^{4}\right], \tag{3.20}$$

where ρ_C is the number of carbon atoms per unit area of the CNT, and is related to the equilibrium bond length of carbon $r_0 = 0.142\,\text{nm}$ by $\rho_C = 4/(3\sqrt{3}r_0^2)\left[R/(R+\Delta R)\right]^2$. The above equation then becomes

$$p = \frac{8\sqrt{2}\pi}{3\sqrt{3}}\left(\frac{R}{R+\Delta R}\right)^2\frac{\varepsilon_{C-H_2}\sigma_{C-H_2}^2}{r_0^2 d_{H_2-H_2}^3}\left[\frac{2}{5}\left(\frac{\sigma_{C-H_2}}{d_{C-H_2}}\right)^{10} - \left(\frac{\sigma_{C-H_2}}{d_{C-H_2}}\right)^{4}\right], \tag{3.21}$$

where the change of CNT radius ΔR and the spacing between hydrogen molecules $d_{H_2-H_2}$ are obtained from Eqs. (3.7) and (3.18), respectively, or from Eqs. (3.12) and (3.19) for small deformation. The spacing d_{C-H_2} is $\sqrt[6]{2/5}\sigma_{C-H_2}$ at the vanishing pressure $p = 0$, and decreases as the pressure p increases, as shown in Fig. 6 for the (5,5) CNT. The atomistic model, also shown in Fig. 6, agrees well with Eq. (3.21) and therefore provides validation.

Eq. (3.21) cannot be solved analytically to give the spacing d_{C-H_2} in terms of the pressure. An approximate but analytical expression can be obtained by neglecting $(\sigma_{C-H_2}/d_{C-H_2})^4$ in Eq. (3.21) since the repulsive term $(\sigma_{C-H_2}/d_{C-H_2})^{10}$ dominates as the internal pressure increases. The spacing d_{C-H_2} can then be approximated by

$$d_{C-H_2} \approx \left[\frac{16\sqrt{2}\pi}{15\sqrt{3}}\left(\frac{R}{R+\Delta R}\right)^2\frac{\varepsilon_{C-H_2}\sigma_{C-H_2}^{12}}{r_0^2 d_{H_2-H_2}^3}\frac{1}{p}\right]^{1/10}. \tag{3.22}$$

3.2.4. *Concentration of hydrogen molecules in a single-wall CNT*

For the CNT of radius $R+\Delta R$, the hydrogen molecules can only be stored within the volume of radius $R + \Delta R - d_{C-H_2}$. The number of hydrogen molecules per unit length of the CNT is $\pi(R + \Delta R - d_{C-H_2})^2\Omega^{-1}$. The number of hydrogen molecules per unit volume of the single-wall CNT is then

$$N_H = \frac{\pi(R+\Delta R - d_{C-H_2})^2\Omega^{-1}}{\pi(R+\Delta R)^2} = \left(\frac{R+\Delta R - d_{C-H_2}}{R+\Delta R}\right)^2\frac{\sqrt{2}}{d_{H_2-H_2}^3}, \tag{3.23}$$

where ΔR, $d_{H_2-H_2}$ and d_{C-H_2} are obtained numerically from Eqs. (3.7), (3.18) and (3.21), respectively. As shown in Fig. 7 for the (5,5) CNT, N_H increases as the internal pressure p increases. The curve stops at the peak pressure $p_{max} = 73.7\,\text{GPa}$ obtained from Fig. 2. This gives the maximum hydrogen storage $31.3\,\text{nm}^{-3}$ in the (5,5) CNT. As shown in Fig. 7, the continuum model agrees reasonably well with the atomistic model, but the latter gives a smaller maximum hydrogen storage $25.6\,\text{nm}^{-3}$ denoted by the rightmost data point.

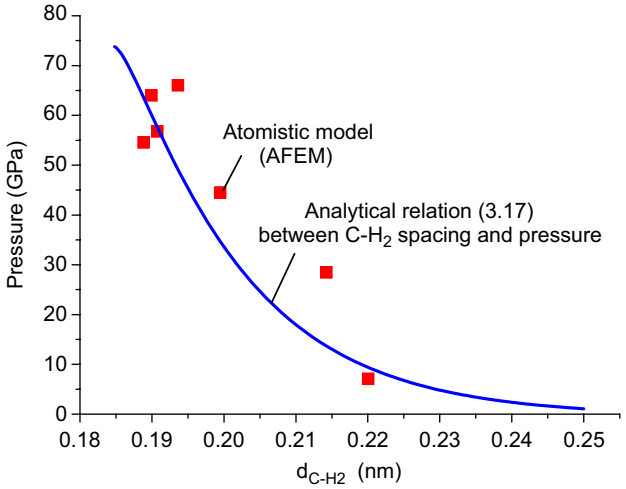

Fig. 6. The pressure inside the single-wall (5,5) carbon nanotube versus the equilibrium spacing between a hydrogen molecule and the nanotube. The results are shown for both the continuum model [Eq. (3.21)] and atomistic model (AFEM).

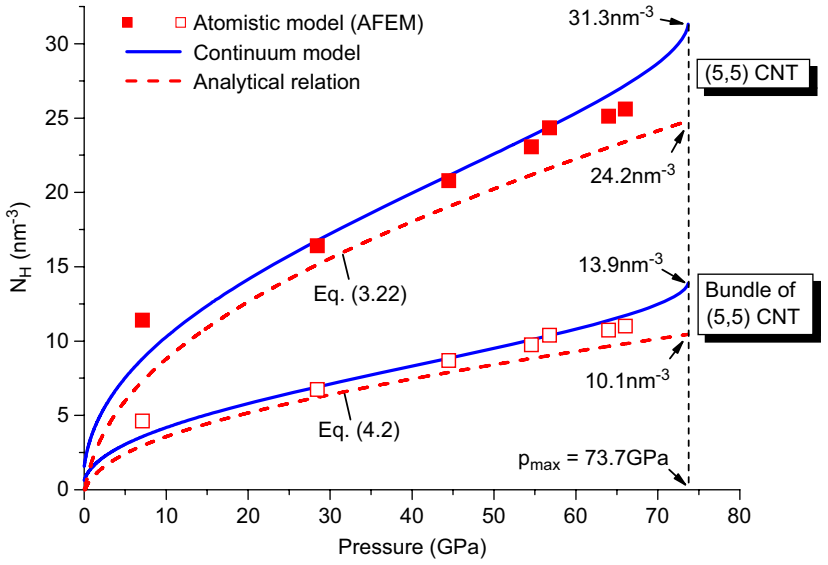

Fig. 7. The number of hydrogen molecules per unit volume versus the pressure inside the single-wall (5,5) carbon nanotubes or their bundles. The results are shown for the continuum model, atomistic model (AFEM) and (approximate) analytical solution [Eq. (3.26) for single-wall carbon nanotubes and Eq. (4.2) for their bundles]. The peak pressure is obtained from Fig. 2 as 73.7 GPa.

For (n,n) armchair CNTs, the CNT radius R is given by

$$R = 0.0678n \text{ (nm)}. \tag{3.24}$$

Similar to Fig. 2, the peak pressure $p_{\max}$ for (n,n) armchair CNTs is also obtained and shown versus the CNT radius R in Fig. 8. It is inversely proportional to R, and is well approximated by

$$p_{\max} = \frac{25.6}{R} \text{ GPa} \cdot \text{nm}. \tag{3.25}$$

The maximum hydrogen storage for the above peak pressure is shown versus the CNT radius R in Fig. 9. It initially increases with R, reaches the peak 65.7 nm^{-3} at the (31,31) CNT ($R = 2.1$ nm), and then decreases gradually. This maximum hydrogen storage (65.7 nm^{-3}) is more than twice of that for the (5,5) CNT, and exceeds the goals of hydrogen storage, as to be discussed in Section 6. However, single-wall CNTs larger than (30,30) may self collapse due to van der Waals interactions (Liu et al., 2004b). Therefore, for hydrogen storage in single-wall CNTs, it is optimal to use the largest one [i.e., (30,30)] without self collapse.

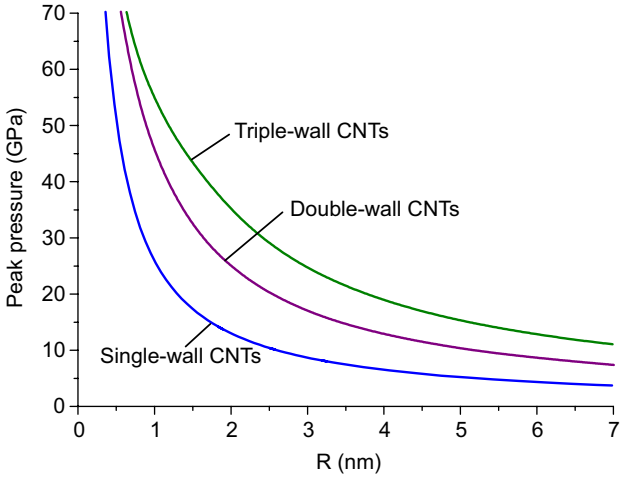

Fig. 8. The peak pressure versus the radius of (inner or innermost) carbon nanotube.

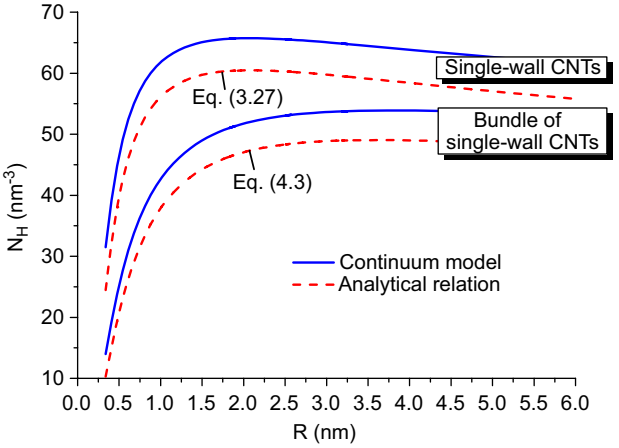

Fig. 9. The maximum hydrogen storage (at the peak pressure) versus the radius of single-wall nanotubes or their bundles. The results are shown for the continuum model and (approximate) analytical solution [Eq. (3.27) for single-wall carbon nanotubes and Eq. (4.3) for their bundles].

3.2.5. *Analytical solution*

The substitution of approximate but analytical relations (3.12), (3.19) and (3.22) into Eq. (3.23) gives the following analytical expression for the number of hydrogen molecules per unit volume of the CNT:

$$N_{\mathrm{H}} = \left(\frac{p}{24\varepsilon_{\mathrm{H_2-H_2}}\sigma^{12}_{\mathrm{H_2-H_2}}}\right)^{1/5}\left[1-\frac{\left(\frac{2}{\sqrt{3}}\right)^{17/50}\left(\frac{\pi}{5r_0^2}\right)^{1/10}\frac{(\varepsilon_{\mathrm{C-H_2}}\sigma^{12}_{\mathrm{C-H_2}})^{1/10}}{(\varepsilon_{\mathrm{H_2-H_2}}\sigma^{12}_{\mathrm{H_2-H_2}})^{1/50}}}{p^{2/25}R\left(1+\frac{pR}{Et}\right)^{6/5}}\right]^2$$

$$= 45.0p^{1/5}\left[1-\frac{0.270}{p^{2/25}R(1+0.00267pR)^{6/5}}\right]^2, \tag{3.26}$$

where Et is given in Eq. (3.11), and the units of p, R and N_{H} are GPa, nm and nm^{-3}, respectively. The above analytical expression, also shown in Fig. 7 for the (5,5) CNT, agrees well with the continuum and atomistic models. [Here, as well as the rest of the paper, "continuum model" refers to the numerical but accurate solution, while "analytical relation" refers to the approximate solution.] The curve also stops at the peak pressure $p_{\max} = 73.7$ GPa obtained from Fig. 2, which gives the maximum hydrogen storage 24.2 nm^{-3} in the (5,5) CNT. It is smaller than 31.3 nm^{-3} given by the continuum model, but is very close to 25.6 nm^{-3} given by the atomistic model.

For other (n,n) armchair CNTs, the substitution of peak pressure in Eq. (3.25) into the above equation gives the maximum hydrogen storage

$$N_{\mathrm{H}} = \frac{86.1}{R^{1/5}}\left(1 - \frac{0.193}{R^{23/25}}\right)^2, \tag{3.27}$$

where the units of R and N_{H} are nm and nm^{-3}, respectively. The above equation gives a maximum hydrogen storage $60.5\,\mathrm{nm}^{-3}$ at the CNT radius $R = 2.1$ nm. As shown in Fig. 9, it is slightly lower than the results from the continuum model, but may have better agreement with the atomistic model.

4. Hydrogen storage in the bundle of single-wall CNTs

The hydrogen storage in single-wall CNTs involves many tubes, which may form CNT bundles. Fig. 10 shows a schematic diagram of an idealized CNT bundle. For relatively large tubes, the equilibrium spacing between CNTs is approximately the same as the characteristic length $\sigma_{\mathrm{C-C}}$ for the van der Waals interactions (Huang et al., 2006; Lu et al., 2007). The number of hydrogen molecules per unit volume of the CNT bundle is then obtained by modifying the volume in Eq. (3.23) as

$$N_{\mathrm{H}} = \frac{\pi(R + \Delta R - d_{\mathrm{C-H_2}})^2 \Omega^{-1}}{2\sqrt{3}\left(R + \Delta R + \dfrac{\sigma_{\mathrm{C-C}}}{2}\right)^2} = \frac{\pi}{2\sqrt{3}}\left(\frac{R + \Delta R - d_{\mathrm{C-H_2}}}{R + \Delta R + \dfrac{\sigma_{\mathrm{C-C}}}{2}}\right)^2 \frac{\sqrt{2}}{d^3_{\mathrm{H_2-H_2}}}. \tag{4.1}$$

It is shown versus the internal pressure p in Fig. 7 for the bundle of (5,5) CNTs. The curve stops at the peak pressure $p_{\max} = 73.7$ GPa. This gives the maximum hydrogen storage in the bundle of (5,5) CNTs as $13.9\,\mathrm{nm}^{-3}$, which is much smaller than $31.3\,\mathrm{nm}^{-3}$ for the (5,5) CNT, and does not reach the goals of hydrogen storage set by the US Department of Energy. As shown in Fig. 7, the continuum model above agrees well with the atomistic model, but overestimates the maximum hydrogen storage since the atomistic model gives $11.0\,\mathrm{nm}^{-3}$ denoted by the rightmost data point. The curves for the CNT bundle are lower than those for single-wall CNTs in Fig. 7 because of the spacing between CNTs in the bundle, which increases the volume for the same number of hydrogen molecules inside CNTs.

Fig. 9 shows the maximum hydrogen storage versus the radius R of the (n,n) armchair CNTs in the bundle. The curve reaches the peak $53.9\,\mathrm{nm}^{-3}$ for the bundle of (55,55) CNTs ($R = 3.73$ nm), which exceeds the goals of hydrogen storage, as to be discussed in Section 6. Since single-wall CNTs larger than the (30,30) CNT may self collapse (Liu et al., 2004b), it is optimal to use the bundle of largest CNTs [i.e., (30,30), $R = 2.1$ nm] without self collapse. The corresponding maximum hydrogen storage is only slightly smaller, $51.9\,\mathrm{nm}^{-3}$.

The substitution of approximate but analytical relations (3.12), (3.19) and (3.22) into Eq. (4.1) gives the following analytical expression for the number of hydrogen molecules per unit volume of the bundle of CNTs:

$$\begin{aligned} N_{\mathrm{H}} &= \frac{\dfrac{\pi}{2\sqrt{3}}\left(\dfrac{p}{24\varepsilon_{\mathrm{H_2-H_2}}\sigma^{12}_{\mathrm{H_2-H_2}}}\right)^{1/5}}{\left(1 + \dfrac{pR}{Et} + \dfrac{\sigma_{\mathrm{C-C}}}{2R}\right)^2}\left\{1 + \frac{pR}{Et} - \frac{\left(\dfrac{2}{\sqrt{3}}\right)^{17/50}\left(\dfrac{\pi}{5r_0^2}\right)^{1/10}\dfrac{(\varepsilon_{\mathrm{C-H_2}}\sigma^{12}_{\mathrm{C-H_2}})^{1/10}}{(\varepsilon_{\mathrm{H_2-H_2}}\sigma^{12}_{\mathrm{H_2-H_2}})^{1/50}}}{p^{2/25}R\left(1 + \dfrac{pR}{Et}\right)^{1/5}}\right\}^2 \\ &= \frac{40.8p^{1/5}}{(R + 0.00267pR^2 + 0.171)^2}\left[R + 0.00267pR^2 - \frac{0.270}{p^{2/25}(1 + 0.00267pR)^{1/5}}\right]^2, \end{aligned} \tag{4.2}$$

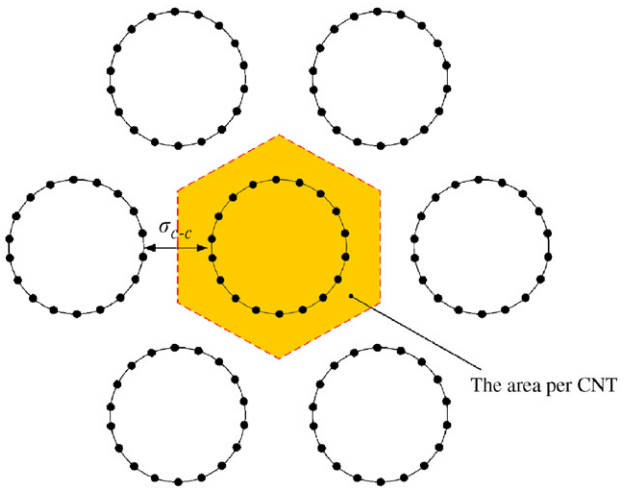

Fig. 10. Schematic diagram of the bundle of single-wall carbon nanotubes.

where Et is given in Eq. (3.11), and the units of p, R and N_H are GPa, nm and nm^{-3}, respectively. The above analytical expression, also shown in Fig. 7 for the bundle of (5,5) CNTs, agrees well with the continuum and atomistic models. The curve also stops at the peak pressure $p_{max} = 73.7$ GPa (from Fig. 2) to give the maximum hydrogen storage 10.1 nm^{-3} in the bundle of (5,5) CNTs, which is smaller than 13.9 nm^{-3} from the continuum model but is close to 11.0 nm^{-3} given by the atomistic model.

For the bundle of (n,n) armchair CNTs, the substitution of peak pressure in Eq. (3.25) into the above equation gives the maximum hydrogen storage

$$N_H = \frac{78.1}{R^{1/5}}\left(1 - \frac{0.206R^{2/25} + 0.171}{1.07R + 0.171}\right)^2, \tag{4.3}$$

where the units of R and N_H are nm and nm^{-3}, respectively. Eq. (4.3) gives a maximum hydrogen storage 49.0 nm^{-3} for the bundle of CNTs with radii $R = 3.6$ nm. As shown in Fig. 9, it is slightly lower than the results from the continuum model, but has better agreement with the atomistic model. For the maximum CNT (30,30) ($R = 2.1$ nm) without self collapse, Eq. (4.3) gives 47.4 nm^{-3}, which is close to 51.9 nm^{-3} given by the continuum model.

5. Hydrogen storage in multi-wall CNTs

5.1. Double-wall CNTs

Fig. 11(a) shows the atomistic model for hydrogen storage in double-wall CNTs of radii R_1 and R_2. The covalent bonds between carbon atoms on the same CNT wall are characterized by the interatomic potential in Eq. (2.1). The carbon atoms from different CNT walls have the van der Waals interactions in Eq. (2.2), and so do carbon atoms and hydrogen molecules inside the CNT.

Fig. 11(b) shows the continuum model to represent the inner and outer CNTs by thin shells of radii R_1 and R_2. The hydrogen molecules are still represented by the internal pressure p (on the inner shell). The van der Waals interaction between shells is characterized by the cohesive law for multi-wall CNTs (Lu et al., 2007), which gives the force–separation relation between two CNT walls from the van der Waals interactions. The equilibrium spacing between CNT walls is the van der Waals parameter σ_{C-C}, i.e., $R_2 = R_1 + \sigma_{C-C}$. Let $R_1 + \Delta R_1$ and $R_2 + \Delta R_2$ denote the radii of inner and outer walls after the internal pressure p is imposed. The energy (per unit length of the CNT) stored between two CNT walls due to van der Waals interactions is (Lu et al., 2007)

$$2\pi^2(R_2 + \Delta R_2 + R_1 + \Delta R_1)\rho_{C_1}\rho_{C_2}\varepsilon_{C-C}\sigma_{C-C}^2\left[\frac{2}{5}\left(\frac{\sigma_{C-C}}{R_2 + \Delta R_2 - R_1 - \Delta R_1}\right)^{10} - \left(\frac{\sigma_{C-C}}{R_2 + \Delta R_2 - R_1 - \Delta R_1}\right)^4\right], \tag{5.1}$$

where ρ_{C_1} and ρ_{C_2} are the numbers of carbon atoms per unit area of the inner and outer CNTs, respectively, and are related to the equilibrium bond length of carbon $r_0 = 0.142$ nm by

$$\rho_{C_i} = \frac{4}{3\sqrt{3}r_0^2}\left(\frac{R_i}{R_i + \Delta R_i}\right)^2 \quad (i = 1, 2).$$

The energy stored in each CNT wall is obtained in the same way as described in Eqs. (3.1)–(3.6). The total energy is the sum of energy in each CNT and the energy between CNT walls in Eq. (5.1) due to van der Waals interactions. The minimization of total energy gives the change of inner and outer CNT radii ΔR_1 and ΔR_2 in terms of the internal pressure p.

Fig. 12 shows the internal pressure p in the CNT versus the percentage of change of CNT radii, $\Delta R_1/R_1$ and $\Delta R_2/R_2$, obtained from both atomistic and continuum models for the (5,5)(10,10) double-wall CNT. The curve for the inner (5,5) CNT is higher than that for the (5,5) single-wall CNT in Fig. 2 due to van der Waals interactions between two CNT walls. The peak pressure for the (5,5)(10,10) double-wall CNT is 89.3 GPa (at which the inner CNT starts to display softening behavior), which is significantly larger than $p_{max} = 73.7$ GPa for the (5,5) single-wall CNT (Fig. 2). The continuum model agrees well with the atomistic model. Only the peak pressure given by the continuum model is slightly higher than the atomistic model.

The analyses in Sections 3.2.2 and 3.2.3 still hold. The spacing between hydrogen molecules $d_{H_2-H_2}$ is determined from Eq. (3.18) [or Eq. (3.19)]. The spacing between the inner CNT wall and nearest hydrogen molecules d_{C-H_2} is obtained from Eq. (3.21) [or Eq. (3.22)] with R and ΔR replaced by R_1 and ΔR_1, respectively.

For the inner CNT of radius $R_1 + \Delta R_1$, the hydrogen molecules can only be stored within the volume of radius $R_1 + \Delta R_1 - d_{C-H_2}$. The number of hydrogen molecules per unit length of the CNT is $\pi(R_1 + \Delta R_1 - d_{C-H_2})^2\Omega^{-1}$. The number of hydrogen molecules per unit volume of the double-wall CNT is then

$$N_H = \frac{\pi(R_1 + \Delta R_1 - d_{C-H_2})^2\Omega^{-1}}{\pi(R_2 + \Delta R_2)^2} = \left(\frac{R_1 + \Delta R_1 - d_{C-H_2}}{R_2 + \Delta R_2}\right)^2\frac{\sqrt{2}}{d_{H_2-H_2}^3}, \tag{5.2}$$

where ΔR_1 and ΔR_2 are determined from the minimization of total energy, and $d_{H_2-H_2}$ and d_{C-H_2} are obtained numerically from Eqs. (3.18) and (3.21), respectively. As shown in Fig. 13 for the (5,5)(10,10) double-wall CNT, N_H increases

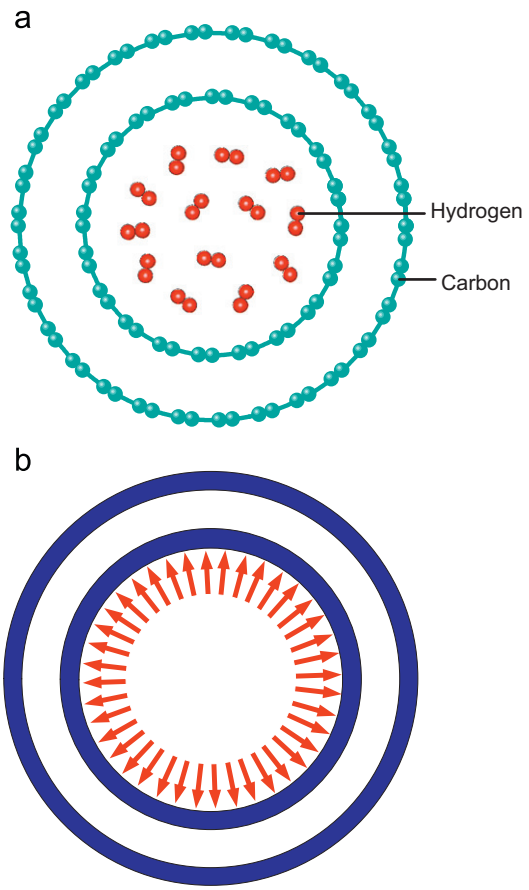

Fig. 11. Schematic diagrams of hydrogen storage in double-wall carbon nanotubes: (a) atomistic model (AFEM), in which carbon atoms and hydrogen molecules are discrete; and (b) continuum model, in which carbon nanotubes are represented by a continuum shell, while hydrogen molecules are represented by the internal pressure.

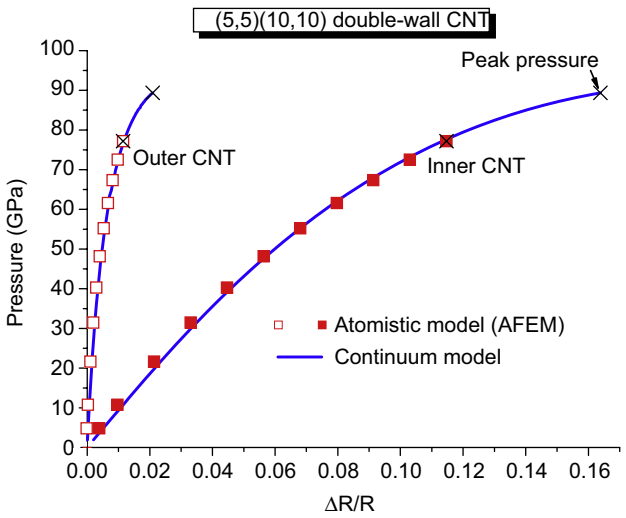

Fig. 12. The pressure inside the (5,5)(10,10) double-wall carbon nanotube versus the percentage change of inner and outer nanotube radii for the atomistic (AFEM) and continuum models. The peak pressure is denoted.

as the internal pressure p increases. The curve stops at the peak pressure 89.3 GPa. This gives the maximum hydrogen storage in the (5,5)(10,10) double-wall CNT as 11.0 nm^{-3}, which is significantly smaller than 31.3 nm^{-3} for (5,5) single-wall CNT and also smaller than 13.9 nm^{-3} for the bundle of (5,5) single-wall CNTs (Fig. 7), and does not

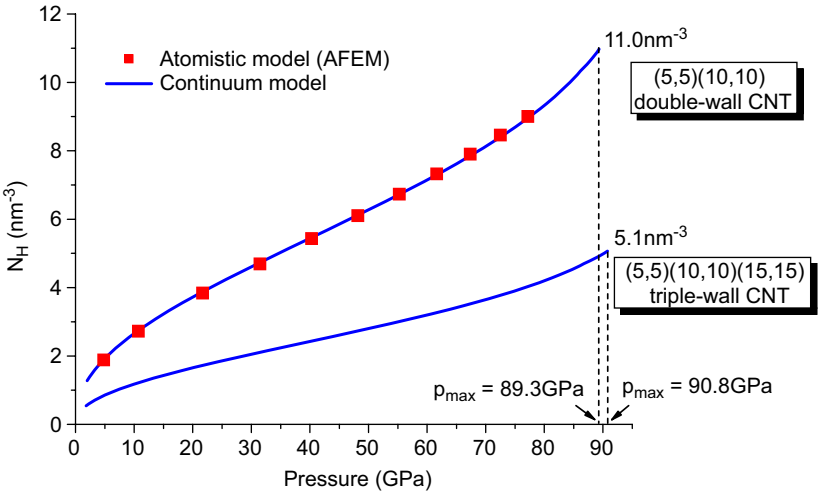

Fig. 13. The number of hydrogen molecules per unit volume versus the pressure inside the (5,5)(10,10) double-wall and (5,5)(10,10)(15,15) triple-wall carbon nanotubes. The results are shown for the continuum model and atomistic model (AFEM). The peak pressures for double- and triple-wall carbon nanotubes are denoted.

reach the goals of hydrogen storage. Fig. 13 also shows the results from the atomistic model, which agree well with the continuum model but give a smaller maximum hydrogen storage 9.0 nm^{-3} denoted by the rightmost data point.

For $(n,n)(n+5,n+5)$ double-wall CNTs, the radii R_1 and R_2 of inner and outer CNTs are still given by Eq. (3.24), and their spacing is approximately σ_{C-C}. The peak pressure p_{max} for double-wall CNTs is shown versus the radius R_1 of the inner CNT in Fig. 8. It is approximately proportional to the inverse of average radius $\bar{R} = (R_1 + R_2)/2$,

$$p_{max} = \frac{48.8}{\bar{R}}\ \text{GPa} \cdot \text{nm}. \tag{5.3}$$

For the above p_{max}, Fig. 14 shows the maximum hydrogen storage versus the inner radius R_1 of double-wall CNT. The curve reaches the peak 63.8 nm^{-3} at the (70,70)(75,75) double-wall CNT ($R_1 = 4.7$ nm). This maximum hydrogen storage is almost six times 11.0 nm^{-3} for the (5,5)(10,10) double-wall CNT, and exceeds the goals of hydrogen storage, as to be discussed in Section 6. However, double-wall CNTs larger than the (36,36)(41,41) CNT may self collapse due to the van der Waals interactions (Xiao et al., 2007). Therefore, for hydrogen storage in double-wall CNTs, it is optimal to use the largest one [i.e., (36,36)(41,41)] without self collapse.

Similar to Section 3.2.1, the change of inner and outer CNT radii ΔR_1 and ΔR_2 can be obtained analytically for small deformation as

$$\begin{Bmatrix} \Delta R_1 \\ \Delta R_2 \end{Bmatrix} = \frac{1}{1 + \lambda(R_1 + R_2)^2} \begin{Bmatrix} 1 + \lambda(R_1 + R_2)R_2 \\ \lambda(R_1 + R_2)R_2 \end{Bmatrix} \frac{pR_1^2}{Et}, \tag{5.4}$$

where $\lambda = 128\pi\varepsilon_{C-C}/(9r_0^4 Et)$ and Et is given in Eq. (3.11). The substitution of the analytical but approximate relations (5.3), (5.4), (3.19) and (3.22) into Eq. (5.2) leads to the following analytical expression for the number of hydrogen molecules per unit volume of double-wall CNT:

$$N_H = 97.9 \frac{(R_1\chi^{6/5} - 0.198\bar{R}^{2/25})^2}{R_2^2\bar{R}^{1/5}\chi^{2/5}\left[1 + 0.0294R_1^2/(1 + 0.448\bar{R}^2)\right]^2}, \tag{5.5}$$

where $\bar{R} = (R_1 + R_2)/2$ is the average radius, $\chi = 1 + 0.130(R_1/\bar{R})(1 + 0.224R_2\bar{R})/(1 + 0.448\bar{R}^2)$, and the units of R_1, R_2, $\bar{R}$ and N_H are nm, nm, nm and nm^{-3}, respectively. Eq. (5.5) gives a maximum hydrogen storage 58.2 nm^{-3} for the inner CNT radius $R_1 = 4.3$ nm. As shown in Fig. 14, it is slightly smaller than that for the continuum model.

5.2. Multi-wall CNTs

The equilibrium spacing between CNT walls is the van der Waals parameter σ_{C-C}, i.e., $R_2 = R_1 + \sigma_{C-C}$, $R_3 = R_2 + \sigma_{C-C}$, … Let $R_1 + \Delta R_1$, $R_2 + \Delta R_2$, $R_3 + \Delta R_3$, … denote the radii of CNT walls after the internal pressure p is imposed. The energy

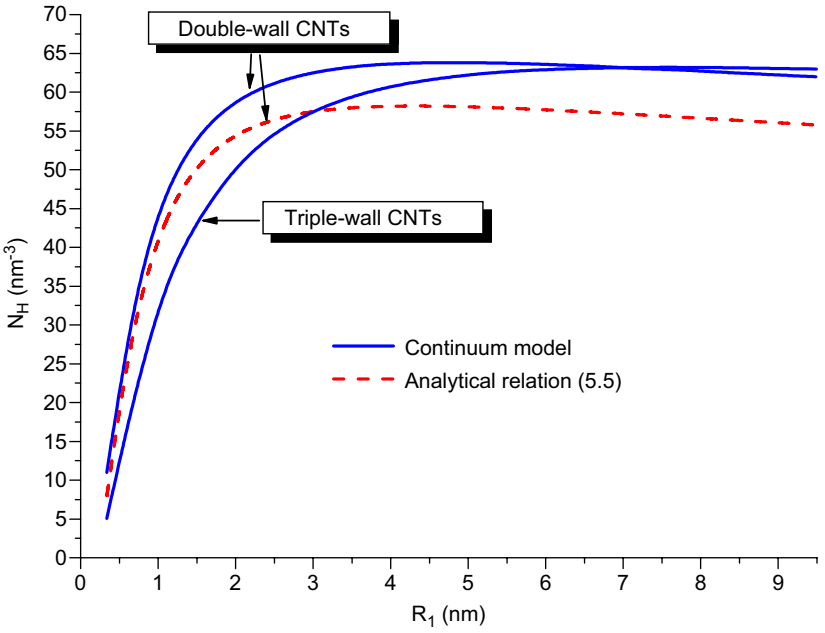

Fig. 14. The maximum hydrogen storage (at the peak pressure) versus the (inner or innermost) radius of double- and triple-wall carbon nanotubes. The results are shown for the continuum model and (approximate) analytical solution [Eq. (5.5)].

(per unit length of the CNT) stored between CNTs walls due to van der Waals interactions is

$$2\pi^2\varepsilon_{\mathrm{C-C}}\sigma_{\mathrm{C-C}}^2\sum_i\left\{\begin{array}{c}(R_{i+1}+\Delta R_{i+1}+R_i+\Delta R_i)\rho_{\mathrm{C}_i}\rho_{\mathrm{C}_{i+1}}\\ \times\left[\frac{2}{5}\left(\frac{\sigma_{\mathrm{C-C}}}{R_{i+1}+\Delta R_{i+1}-R_i-\Delta R_i}\right)^{10}-\left(\frac{\sigma_{\mathrm{C-C}}}{R_{i+1}+\Delta R_{i+1}-R_i-\Delta R_i}\right)^{4}\right]\end{array}\right\},\tag{5.6}$$

where $\rho_{\mathrm{C}_i}=4/\left(3\sqrt{3}r_0^2\right)\left[R_i/(R_i+\Delta R_i)\right]^2$.

The energy stored in each CNT wall is obtained in the same way as described in Eqs. (3.1)–(3.6). The total energy is the sum of energy in each CNT and the energy between CNT walls given in Eq. (5.6) due to van der Waals interactions. The minimization of total energy gives the change of CNT radii ΔR_i ($i=1, 2, 3, \ldots$) in terms of the internal pressure p.

The analyses in Sections 3.2.2 and 3.2.3 still hold. The number of hydrogen molecules per unit volume of the CNT is

$$N_{\mathrm{H}}=\frac{\pi(R_1+\Delta R_1-d_{\mathrm{C-H_2}})^2\Omega^{-1}}{\pi(R_{\mathrm{m}}+\Delta R_{\mathrm{m}})^2}=\left(\frac{R_1+\Delta R_1-d_{\mathrm{C-H_2}}}{R_{\mathrm{m}}+\Delta R_{\mathrm{m}}}\right)^2\frac{\sqrt{2}}{d_{\mathrm{H_2-H_2}}^3},\tag{5.7}$$

where R_{m} is the radius of outermost CNT. It is shown in Fig. 13 versus the internal pressure p for the (5,5)(10,10)(15,15) triple-wall CNT. The peak pressure 90.8 GPa is very close to 89.3 GPa for the (5,5)(10,10) double-wall CNT, which means that the CNTs beyond the innermost two have essentially no effect. The maximum hydrogen storage in the (5,5)(10,10)(15,15) triple-wall CNT is only 5.1 nm^{-3}.

For $(n,n)(n+5,n+5)(n+10,n+10)$ triple-wall CNTs, the peak pressure $p_{\max}$ is shown versus the radius R_1 of the innermost CNT in Fig. 8. It is approximately proportional to the inverse of average radius $\bar{R}=(R_1+R_2+R_3)/3$

$$p_{\max}=\frac{77.3}{\bar{R}}\ \mathrm{GPa}\cdot\mathrm{nm}.\tag{5.8}$$

Fig. 14 shows the maximum hydrogen storage versus R_1. The curve reaches the peak 63.2 nm^{-3} at the (110,110)(115,115)(120,120) triple-wall CNT ($R_1=7.5$ nm). This exceeds the goals of hydrogen storage, as to be discussed in Section 6. However, triple-wall CNTs larger than the (42,42)(47,47)(52,52) CNT may self collapse due to the van der Waals interactions (Xiao et al., 2007). Therefore, for hydrogen storage in triple-wall CNTs, it is optimal to use the largest one [i.e., (42,42)(47,47)(52,52)] without self collapse.

The curve for triple-wall CNTs is lower than its counterpart for double-wall CNTs at the small radius R_1 in Fig. 14, but this trend is reversed at relatively large radius. This is due to two competing effects as the number of walls increases. One is the volume increase (for the same number of hydrogen molecules), which reduces the maximum hydrogen storage. The other is that the peak pressure in the inner(most) wall increases with the increase of number of walls, which allows more hydrogen molecules inside the inner(most) wall. These two effects dominate at small and large radii, respectively, which is

why the curves in Fig. 14 cross. In fact, the comparison of the curve for single-wall CNT in Fig. 9 with the curves for double- and triple-wall CNTs shows the same trend.

6. Discussion and concluding remarks

The maximum hydrogen storage shown in Figs. 9 and 14 corresponds to the limit state at which the (inner or innermost) CNT starts to fracture (or exhibit softening behavior). The strain (in the circumferential direction) is about 16.6%. The cyclic storage and release of hydrogen in CNTs requires the strain be significantly less than this level.

One goal of hydrogen storage set by the US Department of Energy is 62 kg H_2/m^3 of hydrogen (Dillon et al., 1997), which can be converted to $N_H = 18.7\,nm^{-3}$ using the atomic weights. This requires the internal pressure $p = 35.5$ GPa from Fig. 7 for the (5,5) CNT, which corresponds to the strain in the circumferential direction $\varepsilon = \Delta R/R = 4.4\%$. For the bundle of (5,5) CNTs shown in Fig. 7 as well as (5,5)(10,10) double-wall and (5,5)(10,10)(15,15) triple-wall CNTs shown in Fig. 13, the required hydrogen storage $18.7\,nm^{-3}$ can never be reached even when the (inner or innermost) CNT fractures. Fig. 15 shows the strain (in the circumferential direction) in the CNT to achieve 62 kg H_2/m^3 of hydrogen versus n for (n,n) single-wall CNTs and their bundles, $(n,n)(n+5,n+5)$ double-wall and $(n,n)(n+5,n+5)(n+10,n+10)$ triple-wall CNTs. As the CNT radius increases, the strain in the CNT to achieve 62 kg H_2/m^3 decreases. The strain is zero for single-wall CNTs larger than (14,14), which means single-wall CNTs between (14,14) and (30,30) can achieve 62 kg H_2/m^3 without the strain and do not self collapse. For the bundle of CNTs, the strain is zero for CNTs larger than (22,22) such that any bundle of CNTs between (22,22) and (30,30) can achieve 62 kg H_2/m^3 without the strain and do not self collapse. For double-wall CNTs, this range becomes (25,25) to (36,36) (for the inner CNT), while for triple-wall CNTs this range is (37,37) to (42,42) (for the innermost CNT).

For the other goal 6.5wt% of hydrogen storage set by the US Department of Energy (Dillon et al., 1997), the corresponding N_H can be similarly obtained using the atomic weights and CNT radius. Fig. 16 shows the strain (in the circumferential direction) to achieve 6.5 wt% H_2 versus n for (n,n) single-wall CNTs, which is also the same as the bundle of CNTs, and for $(n,n)(n+5,n+5)$ double-wall and $(n,n)(n+5,n+5)(n+10,n+10)$ triple-wall CNTs. As the CNT radius increases, the strain in the CNT to achieve 6.5 wt% H_2 decreases. It is zero for single-wall CNTs (and their bundles) larger than (19,19) such that single-wall CNTs between (19,19) and (30,30) can achieve 6.5 wt% H_2 without the strain and do not self collapse. For double-wall CNTs, this range becomes (32,32) to (36,36) (for the inner CNT), while for triple-wall CNTs this range does not exist anymore.

In order to achieve both goals of 62 kg H_2/m^3 and 6.5 wt% H_2 for hydrogen storage, CNTs display different behavior depending on their radii, as shown in Table 1.

(1) tiny CNTs fracture to reach the goals of hydrogen storage (2nd column);
(2) small CNTs experience strains upon hydrogen storage (3rd column);
(3) medium CNTs have no strain and do not self collapse (4th column); and
(4) large CNTs may self collapse upon the release of hydrogen (5th column).

The corresponding ranges of radii are also shown in Table 1.

For the "small" CNTs in the 3rd column of Table 1, even though the strains are below the fracture strain of CNTs (~16.6%), defects may nucleate in the form of Stone–Wales transformation (90°rotation of a C–C bond) at a much smaller

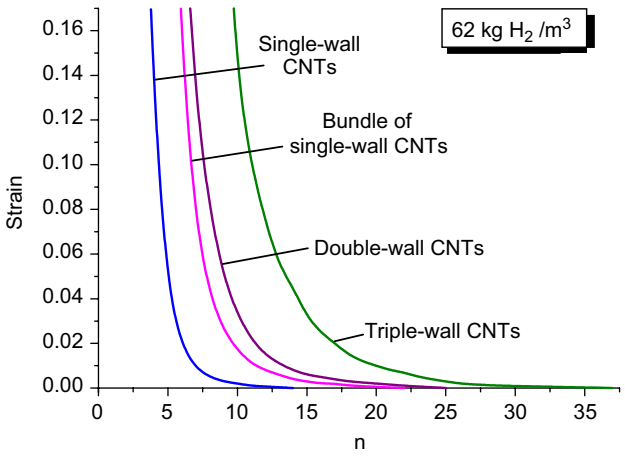

Fig. 15. The strain in the (inner or innermost) carbon nanotube to reach 62 kg H_2/m^3, the goal for hydrogen storage set by the US Department of Energy. The strain is shown versus n for single-, double- and triple-wall carbon nanotubes and their bundles, where (n,n) represent the charality of armchair carbon nanotubes.

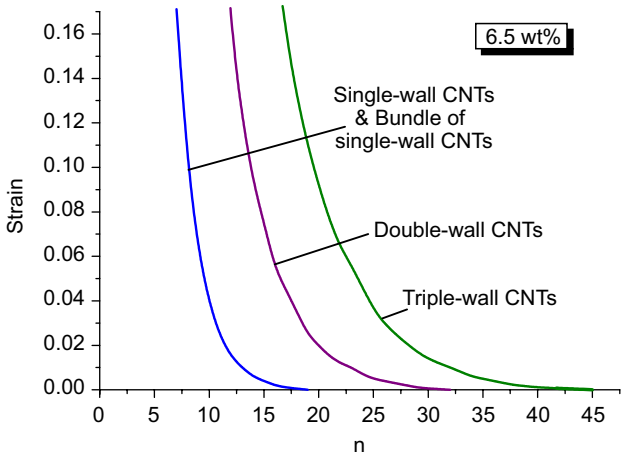

Fig. 16. The strain in the (inner or innermost) carbon nanotube to reach 6.5wt%, the other goal for hydrogen storage set by the US Department of Energy. The strain is shown versus n for single-, double- and triple-wall carbon nanotubes and their bundles, where (n,n) represent the charality of armchair carbon nanotubes.

Table 1
Behavior of different carbon nanotubes to achieve the goals of hydrogen storage (62 kg H_2/m^3 and 6.5 wt%)

	Ranges of CNT charality and radius			
	Fracture	Strained	No strain or self collapse	Self collapse
Single-wall CNTs	(7,7) and down <0.47 nm	(8,8) to (18,18) 0.54–1.2 nm	(19,19) to (30,30) 1.3–2.0 nm	(31,31) and up >2.1 nm
Bundle of single-wall CNTs	(7,7) and down <0.47 nm	(8,8) to (21,21) 0.54–1.4 nm	(22,22) to (30,30) 1.5–2.0 nm	(31,31) and up >2.1 nm
Double-wall CNTs (inner tube)	(11,11) and down <0.75 nm	(12,12) to (31,31) 0.81–2.1 nm	(32,32) to (36,36) 2.2–2.4 nm	(37,37) and up >2.5 nm
Triple-wall CNTs (innermost tube)	(16,16) and down <1.1 nm	(17,17) to (41,41) 1.2–2.8 nm	– –	(42,42) and up >2.8 nm

strain, around 5% (Nardelli et al., 1998a, b; Jiang et al., 2004; Song et al., 2006). Therefore, in order to avoid defect nucleation and self collapse, the suitable ranges for hydrogen storage are (10,10) to (30,30) for single-wall CNTs and their bundles, (17,17) to (36,36) for (the inner tube of) double-wall CNTs, and (24,24) to (41,41) for (the innermost tube of) triple-wall CNTs.

The hydrogen storage in zig–zag and chiral CNTs is also studied. The peak pressure is essentially independent of the charality, and is given by Eqs. (3.25), (5.3) and (5.8) for single-, double- and triple-wall (zig–zag and chiral) CNTs, respectively. For CNTs of the same radius, the maximum hydrogen storage in zig–zag CNTs is a few percent (<5%) higher than that in armchair CNTs, while the results for chiral CNTs are between those for armchair and zig–zag CNTs.

The effect of "caps" at the two ends of the CNT is negligible. The peak pressure for CNTs with closed caps is slightly smaller (less than 1.5%) than that without caps, while the maximum hydrogen storage is less than 0.3% smaller.

Hydrogen adsorption on the exterior surface of CNT is studied by modifying the model shown in Fig. 1 to introduce one layer of hydrogen molecules outside the CNT. The distances between this layer of hydrogen and the CNT and between hydrogen molecules are obtained from Eqs. (3.21) and (3.18) as $d_{C-H_2}|_{p=0} = \sqrt[6]{2/5}\sigma_{C-H_2} = 0.274\,\text{nm}$ and $d_{H_2-H_2}|_{p=0} = \sqrt[6]{2}\sigma_{H_2-H_2} = 0.332\,\text{nm}$, respectively. Fig. 17 shows the maximum hydrogen storage N_H (at the peak internal pressure), with and without surface absorption, versus the CNT radius R for single-wall CNTs. The maximum hydrogen storage with surface absorption is in fact smaller than that without surface absorption because the former occupies a larger volume (corresponding to the radius $R+\Delta R+d_{C-H_2}$, as opposed to $R+\Delta R$ for the latter). This volume increase overwhelms the increase in the number of hydrogen molecules due to surface adsorption, and therefore leads to smaller maximum hydrogen storage.

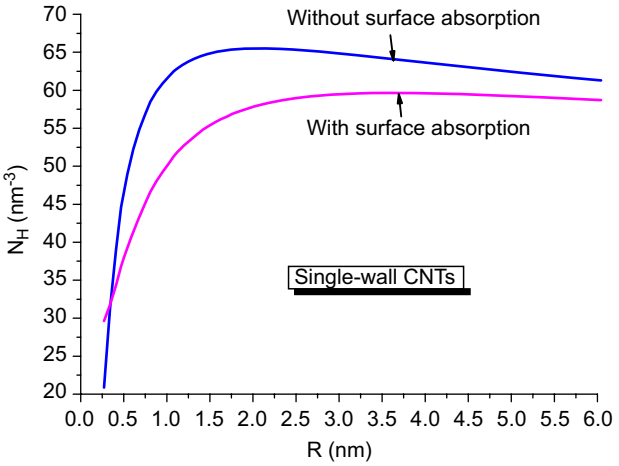

Fig. 17. The maximum hydrogen storage (at the peak pressure) versus the radius of single-wall nanotubes, with and without hydrogen absorption to the exterior surface of nanotubes.

Heterogeneous carbon nanostructures, such as nanotube-derived carbon foam (Ding et al., 2007), CNTs doped by metals (Krasnov et al., 2007), and carbon nano-framework (Weck et al., 2007), have also been studied for hydrogen storage, and so has fullerene (Pupysheva et al., 2008). These heterogeneous carbon nanostructures and fullerene have shown improved hydrogen storage, but are beyond the scope of the present study.

In summary, the following conclusions on hydrogen storage in CNTs are established in this paper.

(1) The continuum models for hydrogen storage in CNTs have been established to account for the deformation of CNTs, the van der Waals interactions between hydrogen molecules and between hydrogen and CNTs. The continuum models agree well with the atomistic simulations without parameter fitting.
(2) For single-, double- and triple-wall CNTs and bundles of single-wall CNTs, the continuum models give analytical expressions of hydrogen storage (number of hydrogen molecules per unit volume) in terms of the CNT radius and pressure. The maximum hydrogen storage corresponding to the peak pressure far exceeds the goals of hydrogen storage ($62\,\mathrm{kg\,H_2/m^3}$ and 6.5wt% H_2) set by the US Department of Energy.
(3) Each type of CNTs (single-, double- and triple-wall, and bundle) can be categorized as tiny, small, medium and large CNTs as shown in Table 1. Tiny CNTs cannot achieve the above goals of hydrogen storage without fracture; small CNTs are strained during hydrogen storage; medium CNTs can achieve the above goals without the strain and do not self collapse; and large CNTs may self collapse upon the release of hydrogen.

Acknowledgments

B.L. acknowledges the support from National Natural Science Foundation of China (Grant nos. 10542001, 10702034 and 10732050). K.C.H. acknowledges the support from National Basic Research Program of China (973 Program) Grant no. 2007CB936803. Y.H. acknowledges the support from the NSF through Nano-CEMMS (Grant no. DMI03-28162) at the University of Illinois and ONR Composites for Marine Structures Program (Grant no. N00014-01-1-0205, Program Manager Dr. Y.D.S. Rajapakse). The supports from the NSFC and Ministry of Education of China are also acknowledged.

References

Allen, M.P., Tildesley, D.J., 1987. Computer Simulation of Liquids. Clarendon Press, Oxford.
Born, M., Huang, K., 1954. Dynamical Theory of the Crystal Lattices. Oxford University Press, Oxford.
Brenner, D.W., Shenderova, O.A., Harrison, J.A., Stuart, S.J., Ni, B., Sinnott, S.B., 2002. A second-generation reactive empirical bond order (REBO) potential energy expression for hydrocarbons. J. Phys.: Condens. Matter 14, 783–802.
Chen, P., Wu, X., Lin, J., Tan, K.L., 1999. High H_2 uptake by alkali-doped carbon nanotubes under ambient pressure and moderate temperatures. Science 285 (5424), 91–93.
Cheng, H.-M., Yang, Q.-H., Liu, C., 2001. Hydrogen storage in carbon nanotubes. Carbon 39 (10), 1447–1454.
Cheng, J., Yuan, X., Zhao, L., Huang, D., Zhao, M., Dai, L., Ding, R., 2004. GCMC simulation of hydrogen physisorption on carbon nanotubes and nanotube arrays. Carbon 42 (10), 2019–2024.
Dai, G.P., Liu, C., Liu, M., Wang, M.Z., Cheng, H.M., 2002. Electrochemical hydrogen storage behavior of ropes of aligned single-walled carbon nanotubes. Nano Letters 2 (5), 503–506.
Darkrim, F.L., Levesque, D., 1998. Monte Carlo simulations of hydrogen adsorption in single-walled carbon nanotubes. J. Chem. Phys. 109 (12), 4981–4984.
Darkrim, F.L., Levesque, D., 2000. High adsorptive property of opened carbon nanotubes at 77 K. J. Phys. Chem. 104, 6773–6776.
Darkrim, F.L., Malbrunot, P., Tartaglia, G.P., 2002. Review of hydrogen storage by adsorption in carbon nanotubes. Int. J. Hydrogen Energy 27 (2), 193–202.
Dillon, A.C., Jones, K.M., Bekkedahl, T.A., Kiang, C.H., Bethune, D.S., Heben, M.J., 1997. Storage of hydrogen in single-walled carbon nanotubes. Nature 386, 377–379.

Ding, F., Lin, Y., Krasnov, P.O., Yakobson, B.I., 2007. Nanotube-derived carbon foam for hydrogen sorption. J. Chem. Phys. 127 (16), 164703.
Dodziuk, H., Dolgonos, G., 2002. Molecular modeling study of hydrogen storage in carbon nanotubes. Chem. Phys. Lett. 356 (1–2), 79–83.
Frankland, S.J.V., Harik, V.M., Odegard, G.M., Brenner, D.W., Gates, T.S., 2003. The stress–strain behavior of polymer–nanotube composites from molecular dynamics simulation. Compos. Sci. Technol. 63, 1655–1661.
Gao, H.J., Klein, P., 1998. Numerical simulation of crack growth in an isotropic solid with randomized internal cohesive bonds. J. Mech. Phys. Solids 46, 187–218.
Gu, C., Gao, G.-H., Yu, Y.-X., Mao, Z.-Q., 2001. Simulation study of hydrogen storage in single walled carbon nanotubes. Int. J. Hydrogen Energy 26 (7), 691–696.
Huang, Y., Wu, J., Hwang, K.C., 2006. Thickness of graphene and single-wall carbon nanotubes. Phys. Rev. B 74, (245413/1–9).
Jiang, H., Feng, X.Q., Huang, Y., Hwang, K.C., Wu, P.D., 2004. Defect nucleation in carbon nanotubes under tension and torsion: Stone–Wales transformation. Comput. Methods Appl. Mech. Eng. 193 (30–32), 3419–3429.
Jiang, L.Y., Huang, Y., Jiang, H., Ravichandran, G., Gao, H., Hwang, K.C., Liu, B., 2006. A cohesive law for carbon nanotube/polymer interfaces based on the van der Waals force. J. Mech. Phys. Solids 54, 2436–2452.
Krasnov, P.O., Ding, F., Singh, A.K., Yakobson, B.I., 2007. Clustering of Sc on SWNT and reduction of hydrogen uptake: ab-initio all-electron calculations. J. Phys. Chem. C 111 (49), 17977–17980.
Liu, B., Huang, Y., Jiang, H., Qu, S., Hwang, K.C., 2004a. The atomic-scale finite element method. Comput. Methods Appl. Mech. Eng. 193, 1849–1864.
Liu, B., Yu, M.F., Huang, Y.G., 2004b. Role of lattice registry in the full collapse and twist formation of carbon nanotubes. Phys. Rev. B 70 (16), 161402.
Liu, B., Jiang, H., Huang, Y., Qu, S., Yu, M.-F., 2005. Atomic-scale finite element method in multiscale computation with applications to carbon nanotubes. Phys. Rev. B 72 (3), (035435/1–8).
Liu, C., Fan, Y.Y., Liu, M., Cong, H.T., Cheng, H.M., Dresselhaus, M.S., 1999. Hydrogen storage in single-walled carbon nanotubes at room temperature. Science 286 (5442), 1127–1129.
Lu, W.B., Wu, J., Jiang, L.Y., Huang, Y., 2007. A cohesive law for multi-wall carbon nanotubes. Philos. Mag. 87, 2221–2232.
McLellan, A.G., 1974. Virial theorem generalized. Am. J. Phys. 42, 239–243.
Mu, S.-c., Tang, H.-l., Qian, S.-h., Pan, M., Yuan, R.-z., 2006. Hydrogen storage in carbon nanotubes modified by microwave plasma etching and Pd decoration. Carbon 44 (4), 762–767.
Nardelli, M.B., Yakobson, B.I., Bernholc, J., 1998a. Brittle and ductile behavior in carbon nanotubes. Phys. Rev. Lett. 81, 4656–4659.
Nardelli, M.B., Yakobson, B.I., Bernholc, J., 1998b. Mechanism of strain release in carbon nanotubes. Phys. Rev. B 57, R4277–R4280.
Pupysheva, O.V., Farajian, A.A., Yakobson, B.I., 2008. Fullerene nanocage capacity for hydrogen storage. Nano Letters 8 (3), 767–774.
Rajalakshmi, N., Dhathathreyan, K.S., Govindaraj, A., Satishkumar, B.C., 2000. Electrochemical investigation of single-walled carbon nanotubes for hydrogen storage. Electrochim. Acta 45, 4511–4515.
Rowlinson, J.S., Widom, B., 1982. Molecular Theory of Capillarity. Clarendon Press, Oxford.
Song, J., Jiang, H., Shi, D.L., Feng, X.Q., Huang, Y., Yu, M.F., Hwang, K.C., 2006. Stone–Wales transformation: precursor of fracture in carbon nanotubes. Int. J. Mech. Sci. 48 (12), 1464–1470.
Timoshenko, S., Goodier, J.N., 1969. Theory of Elasticity, third ed. McGraw-Hill Book Co., Inc., New York.
Tsai, D.H., 1979. The virial theorem and stress calculation in molecular dynamics. J. Chem. Phys. 70 (3), 1375–1382.
Weck, P.F., Kim, E., Balakrishnan, N., Cheng, H.S., Yakobson, B.I., 2007. Designing carbon nanoframeworks tailored for hydrogen storage. Chem. Phys. Lett. 439, 354–359.
Wu, J., Hwang, K.C., Huang, Y., 2008. An atomistic-based finite-deformation shell theory for single-wall carbon nanotubes. J. Mech. Phys. Solids 56, 279–292.
Wu, X.B., Chen, P., Lin, J., Tan, K.L., 2000. Hydrogen uptake by carbon nanotubes. Int. J. Hydrogen Energy 25 (3), 261–265.
Xiao, J., Liu, B., Huang, Y., Zuo, J., Hwang, K.C., Yu, M.F., 2007. Collapse and stability of single- and multi-wall carbon nanotubes. Nanotechnology 18, 395703.
Yang, R.T., 2000. Hydrogen storage by alkali-doped carbon nanotubes—revisited. Carbon 38, 623–626.
Ye, Y., Ahn, C.C., Witham, C., Fultz, B., Liu, J., Rinzler, A.G., Colbert, D., Smith, K.A., Smalley, R.E., 1999. Hydrogen adsorption and cohesive energy of single-walled carbon nanotubes. Appl. Phys. Lett. 74 (16), 2307–2309.
Zhang, P., Huang, Y., Geubelle, P.H., Klein, P.A., Hwang, K.C., 2002. The elastic modulus of single-wall carbon nanotubes: a continuum analysis incorporating interatomic potentials. Int. J. Solid Struct. 39, 3893–3906.
Zhang, P., Jiang, H., Huang, Y., Geubelle, P.H., Hwang, K.C., 2004. An atomistic-based continuum theory for carbon nanotubes: analysis of fracture nucleation. J. Mech. Phys. Solids 52, 977–998.